nature communications

Article

https://doi.org/10.1038/s41467-023-44520-4

Amyloid beta 42 alters cardiac metabolism and impairs cardiac function in male mice with obesity

Received: 18 October 2023

Accepted: 15 December 2023

Published online: 15 January 2024

Check for updates

Liam G. Hall[1,2,10], Juliane K. Czeczor[1,3,10], Timothy Connor[1], Javier Botella[1], Kirstie A. De Jong[1,4], Mark C. Renton[5], Amanda J. Genders[1,6], Kylie Venardos[1], Sheree D. Martin[1], Simon T. Bond[1,7], Kathryn Aston-Mourney[1], Kirsten F. Howlett[5], James A. Campbell[8], Greg R. Collier[8], Ken R. Walder[1], Matthew McKenzie[9], Mark Ziemann[9] & Sean L. McGee[1,8]

There are epidemiological associations between obesity and type 2 diabetes, cardiovascular disease and Alzheimer's disease. The role of amyloid beta 42 ($A\beta_{42}$) in these diverse chronic diseases is obscure. Here we show that adipose tissue releases $A\beta_{42}$, which is increased from adipose tissue of male mice with obesity and is associated with higher plasma $A\beta_{42}$. Increasing circulating $A\beta_{42}$ levels in male mice without obesity has no effect on systemic glucose homeostasis but has obesity-like effects on the heart, including reduced cardiac glucose clearance and impaired cardiac function. The closely related $A\beta_{40}$ isoform does not have these same effects on the heart. Administration of an Aβ-neutralising antibody prevents obesity-induced cardiac dysfunction and hypertrophy. Furthermore, Aβ-neutralising antibody administration in established obesity prevents further deterioration of cardiac function. Multi-contrast transcriptomic analyses reveal that $A\beta_{42}$ impacts pathways of mitochondrial metabolism and exposure of cardiomyocytes to $A\beta_{42}$ inhibits mitochondrial complex I. These data reveal a role for systemic $A\beta_{42}$ in the development of cardiac disease in obesity and suggest that therapeutics designed for Alzheimer's disease could be effective in combating obesity-induced heart failure.

Epidemiological evidence has identified associations between obesity, Alzheimer's disease (AD) and cardiovascular disease[1–3]. Common underlying aetiological factors such as inflammation, hypertension and hormonal alterations have all been implicated, however, the exact mechanisms involved remain largely unexplored. Another potential molecular link are amyloid beta peptides (Aβ), a putative pathogenic driver of AD[4]. Aβ peptides, ranging from 36-44 amino acids in length, are derived by proteolytic processing of the trans-membrane amyloid precursor protein (APP)[5]. Initial cleavage by either α- or β-secretases commits APP to the non-amyloidogenic or amyloidogenic pathways,

[1]Institute for Mental and Physical Health and Clinical Translation, Metabolic Research Unit, School of Medicine, Deakin University, Geelong, Australia. [2]Department of Cellular and Physiological Sciences, Faculty of Medicine, The University of British Columbia, Vancouver, Canada. [3]Becton Dickinson GmbH, Medical Affairs, 69126 Heidelberg, Germany. [4]Institute of Experimental Cardiovascular Research, University Medical Centre Hamburg-Eppendorf, Hamburg, Germany. [5]Institute for Physical Activity and Nutrition, School of Exercise and Nutrition Sciences, Deakin University, Geelong, Australia. [6]Department of Nutrition, Dietetics and Food, School of Clinical Sciences and Victorian Heart Institute, Monash University, Melbourne, Australia. [7]Baker Heart and Diabetes Institute, Melbourne, Australia. [8]Ambetex Pty Ltd, Geelong, Australia. [9]School of Life and Environmental Science, Deakin University, Geelong, Australia. [10]These authors contributed equally: Liam G. Hall, Juliane K. Czeczor. e-mail: sean.mcgee@deakin.edu.au

respectively[5]. Following cleavage by the β-secretase BACE1, the remaining β-C-terminal fragment of APP can be cleaved by γ-secretase, which produces Aβ peptides that are released into the extracellular space via exocytosis[5]. Aβ peptides of 40 and 42 amino acids ($Aβ_{40}$ and $Aβ_{42}$) are the most common and $Aβ_{42}$ has a particular propensity to aggregate and form oligomers[4]. The oligomerisation state of $Aβ_{42}$, which is highly dynamic and stochastic, impacts its function and ability to interact with numerous cell surface receptors[6–8]. Extracellular $Aβ_{42}$ can also be internalised and interact with organelles, intracellular signalling molecules and enzymes, disrupting normal cellular function[9].

Accumulation of $Aβ_{42}$ in the central nervous system is linked with alterations in metabolism, including impairments in glucose uptake[10,11], glucose utilisation[12] and aspects of mitochondrial function[13–16] in several different cell types. APP and its proteolytic processing pathways are expressed in peripheral tissues and Aβ peptides are found in plasma[17]. The expression of APP is increased in adipose tissue of humans affected by obesity[18] and APP overexpression in adipose tissue of mice causes adiposity and insulin resistance due to impaired adipocyte mitochondrial function[19]. Circulating concentrations of $Aβ_{42}$ correlate with fat mass, however whether circulating $Aβ_{42}$ regulates peripheral metabolism, particularly in the context of obesity, remains largely unexplored. This study aimed to determine whether $Aβ_{42}$ is released by adipose tissue and whether this is increased in obesity. Finally, this study also sought to determine the metabolic consequences of persistently increased circulating levels of $Aβ_{42}$. Here we show that adipose tissue releases $Aβ_{42}$, which is increased in obesity and associates with higher plasma $Aβ_{42}$. We also show that increases in plasma $Aβ_{42}$ negatively impact cardiac metabolism and function and that $Aβ_{42}$ accumulates in cardiac mitochondria and inhibits complex I of the respiratory chain. Antagonising $Aβ_{42}$ with a neutralising antibody prevents obesity-induced defects in cardiac function and prevents further decline of cardiac function in established obesity. These findings enhance our understanding of the impact of obesity on the heart and provide a rationale for the repurposing of AD therapies for the treatment of heart failure.

Results

$Aβ_{42}$ is released from adipose tissue, which is increased in obesity

To better understand the proteolytic processing of APP in the periphery in obesity, the expression and activity of APP and components of the amyloidogenic pathway were assessed in tissues from control and diet-induced obese mice, which had increased total fat mass and increased mass of individual fat pads (Supplementary Fig. 1a, b). The expression of *App* was increased in adipose tissue of obese mice, but not in the liver or skeletal muscle (Fig. 1a). Similarly, *Bace1* (Fig. 1b) and *Psen1* (Fig. 1c), which encodes the presenilin 1 subunit of γ-secretase, were also increased in adipose tissue of obese mice, but not in the liver or skeletal muscle. The activity of BACE1 was increased in adipose tissue and reduced in the liver of obese mice (Fig. 1d). Adipose tissue explants were found to release both $Aβ_{40}$ and $Aβ_{42}$ but this was not different between control and obese mice when expressed relative to explant mass (Fig. 1e). However, when accounting for total fat pad mass, adipose tissue of obese mice released more $Aβ_{40}$ and $Aβ_{42}$ (Fig. 1f). Release of $Aβ_{42}$ was inhibited by incubation of explants with Brefeldin A (BFA; Supplementary Fig. 1c), an inhibitor of exocytosis[20], indicating that adipose tissue actively secretes Aβ isoforms. The plasma concentration of $Aβ_{42}$, but not $Aβ_{40}$, was elevated in obese mice (Fig. 1g). Similar to findings in humans[21], plasma $Aβ_{42}$ was significantly correlated with fat mass (Supplementary Fig. 1d) but not with lean mass (Supplementary Fig. 1e). Together these data show that Aβ isoforms are released from adipose tissue, which is associated with elevated circulating $Aβ_{42}$ in obesity.

$Aβ_{42}$ administration reprograms cardiac glucose metabolism

To examine the effect of increased circulating $Aβ_{42}$ on systemic metabolism, mice were administered $Aβ_{42}$ or a peptide corresponding to a scrambled $Aβ_{42}$ sequence ($ScrAβ_{42}$; 1μg/day i.p.) for 4 weeks

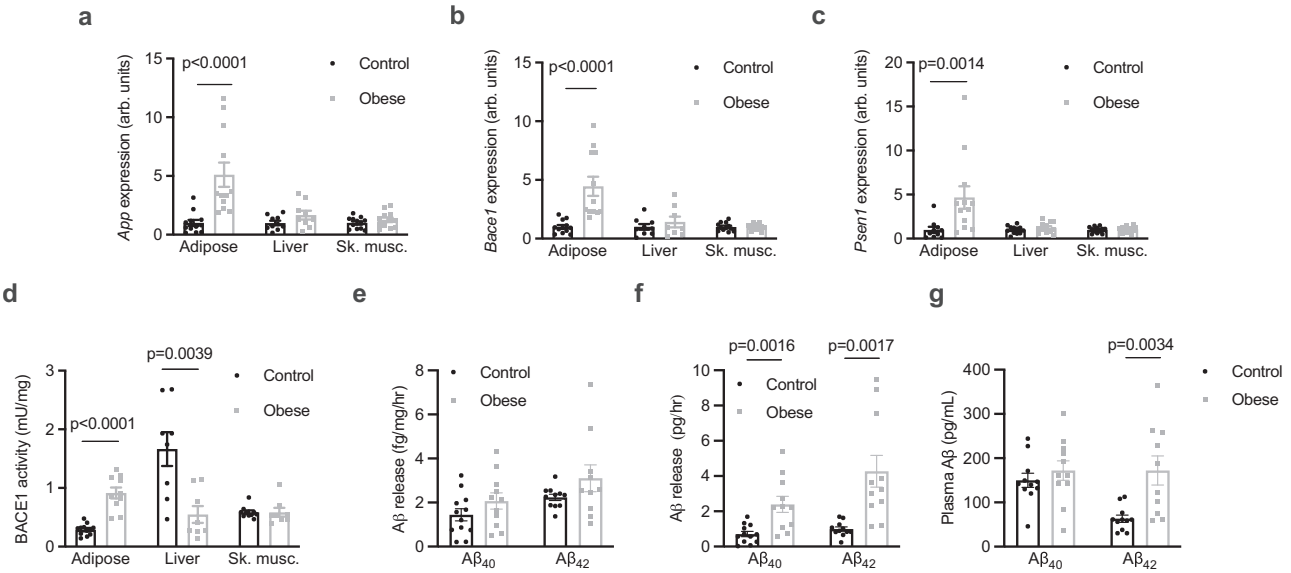

Fig. 1 | Ab_{42} is released from adipose tissue, which is increased in obesity. a *App* expression in adipose tissue (Mann Whitney test, U = 6; n = 12/group), the liver (n = 10 and 9/group respectively) and skeletal muscle (Sk. musc., quadriceps; unpaired t-tests; n = 12/group) from control and obese mice. **b** *Bace1* expression in adipose tissue (Mann Whitney test, U = 1; n = 12/group), the liver (n = 9 and 8/group, respectively) and sk. musc. (unpaired t-tests; n = 12/group) from control and obese mice. **c,** *Psen1* expression in adipose tissue (Mann Whitney test, U = 14; n = 10 and 12/group respectively), the liver (n = 12/group) and sk. musc. (n = 12/group) from control and obese mice (unpaired t-tests). **d** BACE1 activity in adipose tissue (n = 12 and 10/group respectively), the liver (n = 8/group) and sk. musc. (n = 8/group) from control and obese mice (unpaired t-tests). **e** relative release of Aβ isoforms from adipose tissue of control and obese mice normalised for tissue weight. **f** absolute release of Aβ isoforms from adipose tissue of control (n = 12) and obese (n = 11) mice (Mann Whitney test, U = 6). **g** plasma Aβ isoforms in control (n = 12) and obese (n = 11) mice (unpaired t-test). All data are mean ± SEM. Statistical tests are two-tailed. Source data are provided in the Source Data file.

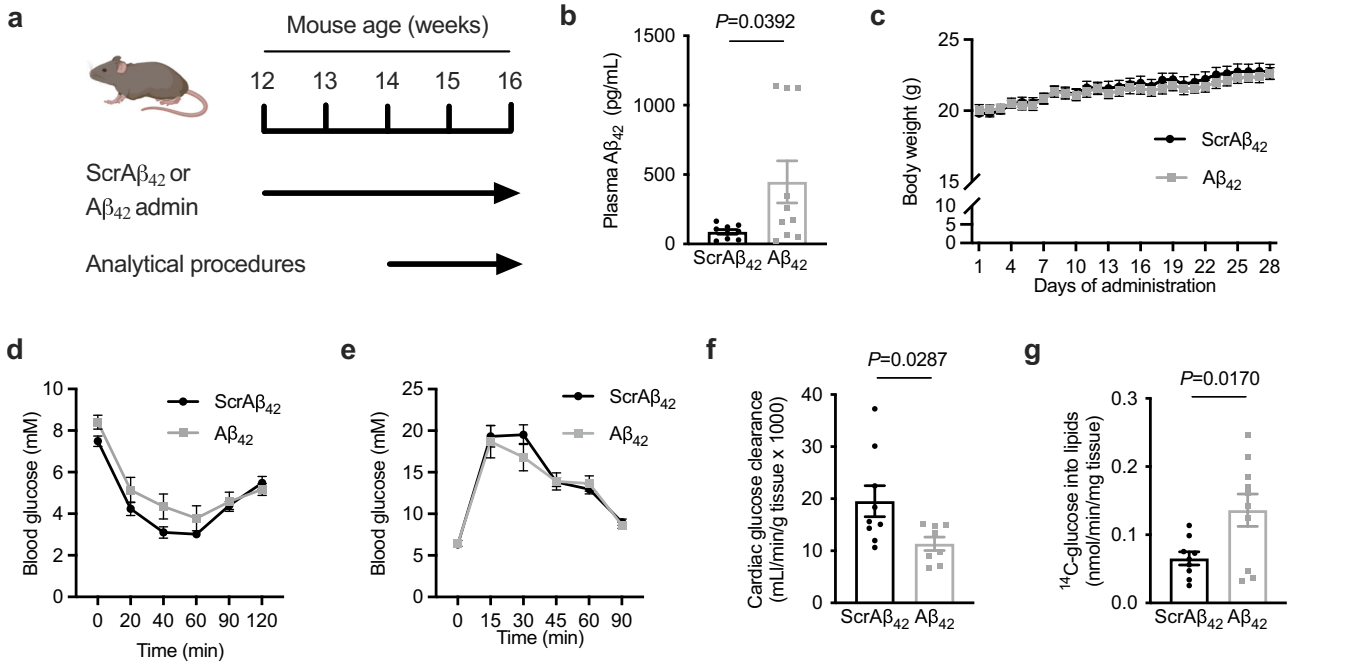

Fig. 2 | Aβ42 administration reprograms cardiac metabolism. a schematic of experiment where mice were administered $Aβ_{42}$ or scrambled $Aβ_{42}$ ($ScrAβ_{42}$; 1 µg/day i.p.) for 4 weeks and analytical procedures were performed in final two weeks. **b** plasma $Aβ_{42}$ in mice 5 h after administration of $ScrAβ_{42}$ ($n = 9$) or $Aβ_{42}$ ($n = 10$; unpaired t-test). **c** body weight in mice administered $ScrAβ_{42}$ or $Aβ_{42}$. ($n = 10$/group). **d** blood glucose during an insulin tolerance test in mice administered $ScrAβ_{42}$ or $Aβ_{42}$ ($n = 10$/group). **e**, blood glucose during a glucose tolerance test in mice administered $ScrAβ_{42}$ or $Aβ_{42}$ ($n = 10$/group). **f** cardiac glucose clearance in mice administered $ScrAβ_{42}$ ($n = 10$) or $Aβ_{42}$ ($n = 9$; unpaired t-test). **g** ^{14}C-glucose incorporation into lipids in mice administered $ScrAβ_{42}$ ($n = 9$) or $Aβ_{42}$ ($n = 10$; unpaired t-test). All data are mean ± SEM. Statistical tests are two-tailed. Source data are provided in the Source Data file. Elements of **a** are created with BioRender.com.

(Fig. 2a). Recombinant human $Aβ_{42}$ was used as it has a greater propensity to aggregate than the mouse sequence and is more likely to reveal any pathological effects of raised $Aβ_{42}$ concentrations[22]. These $Aβ_{42}$ peptides appeared as monomers and low molecular weight aggregates by SDS-PAGE (Supplementary Fig. 2a). This administration regimen increased plasma $Aβ_{42}$ ~ 4-fold (Fig. 2b) but had no effect on body weight (Fig. 2c) or composition (Supplementary Fig. 2b, c). Similarly, $Aβ_{42}$ administration had no effect on blood glucose during both insulin (Fig. 2d) and glucose tolerance tests (GTT; Fig. 2e), or on glucose-stimulated insulin secretion (Supplementary Fig. 2d). However, further analysis of glucose fate throughout the GTT using both 2-^{2}H-deoxyglucose and 1-^{14}C-glucose tracers revealed that glucose clearance by the heart was reduced in mice administered $Aβ_{42}$ (Fig. 2f). In contrast, there were no differences in glucose clearance by skeletal muscle or adipose tissue (Supplementary Fig. 2e). Furthermore, in mice administered $Aβ_{42}$ glucose incorporation into lipids was increased (Fig. 2g), which was associated with a trend ($p = 0.0830$) towards increased cardiac triglycerides (TG; Supplementary Fig. 2f). These alterations in cardiac metabolism in mice administered $Aβ_{42}$ were independent of changes in plasma free fatty acids and lipids (Supplementary Fig. 2g–j). These data show that increasing systemic $Aβ_{42}$ alters cardiac glucose metabolism.

Aβ42 administration induces cardiac dysfunction

Obesity results in reprogramming of cardiac metabolism that includes impaired glucose uptake and oxidation for a given insulin concentration[23]. These alterations in cardiac metabolism have been linked to impairments in cardiac relaxation and left ventricular (LV) filling[24]. Although increased filling pressures can overcome this diastolic dysfunction in early phases of the disease[25], longer-term consequences include LV hypertrophy and eventual heart failure[25]. This form of heart failure most commonly manifests as heart failure with preserved ejection fraction (HFpEF)[25,26]. Hence, obesity-induced alteration of cardiac metabolism is a precipitating event leading to obesity-induced heart failure[24,25]. Given the effect of $Aβ_{42}$ on cardiac metabolism, the effect of $Aβ_{42}$ on cardiac function was examined by echocardiography (Supplementary Fig. 3a). Administration of $Aβ_{42}$ had wide-ranging effects on cardiac function, including impaired diastolic function, represented by increased deceleration time (Fig. 3a) and reduced E:A ratio (Fig. 3b), indicating impairments in cardiac relaxation. Furthermore, mice administered $Aβ_{42}$ displayed evidence of impaired systolic function, including reduced ejection fraction (Fig. 3c) and fractional shortening (Fig. 3d). Mice administered $Aβ_{42}$ had largely normal cardiac morphology when compared with mice administered $ScrAβ_{42}$ (Supplementary Table 1). To better understand how $Aβ_{42}$ impairs cardiac function, profiling of genes that are differentially expressed in human heart failure specifically in the major cell types of the heart[27] was performed. In hearts of mice administered $Aβ_{42}$, there was a significant increase in the expression of *Nppa* (Fig. 3e), which encodes natriuretic peptide A, and is increased in cardiomyocytes in human heart failure[27]. In contrast, there were no changes in the expression of *Fap, Itga1, Rora* and *Fgfr1*, which are increased in heart failure in cardiac fibroblasts, pericytes, smooth myocytes and endothelial cells, respectively[27]. Together, these data indicate that $Aβ_{42}$ impairs cardiac function, likely through effects on cardiomyocytes.

In the context of AD, $Aβ_{42}$ is considered the most pathogenic of the Aβ peptides because of its propensity to aggregate[28]. However, $Aβ_{40}$ is also found in plasma[17,29]. To determine whether $Aβ_{40}$ also has deleterious effects on the heart, mice were administered $Aβ_{40}$ (1µg/day i.p.) for 4 weeks followed by echocardiographic assessment of cardiac function and morphology, as was performed for $Aβ_{42}$. Administration of $Aβ_{40}$ markedly increased the circulating concentration of $Aβ_{40}$ (Supplementary Fig. 3b) but had no effect on body weight and composition (Supplementary Fig. 3c–e), and had no effect on any index of cardiac function or morphology (Supplementary Table 2 and

https://doi.org/10.1038/s41467-023-44520-4

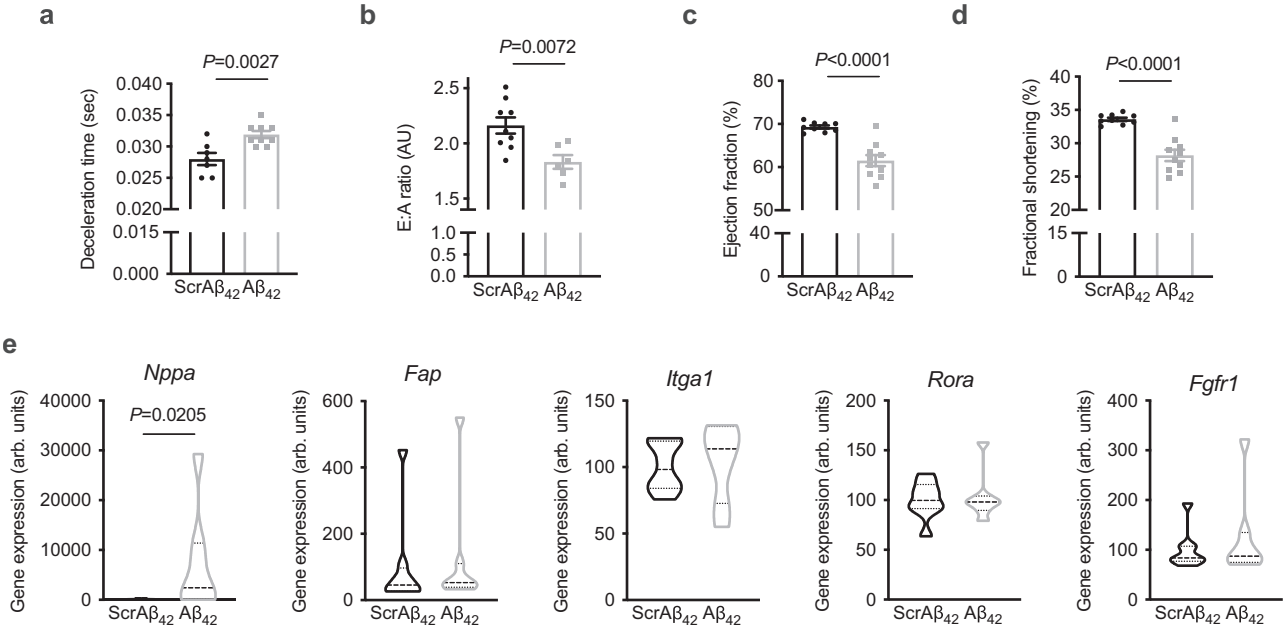

Fig. 3 | $A\beta_{42}$ administration induces cardiac dysfunction. a deceleration time in mice administered $ScrA\beta_{42}$ or $A\beta_{42}$ (unpaired t-test; $n = 7$ and 9/group respectively). **b** E:A ratio in mice administered $ScrA\beta_{42}$ or $A\beta_{42}$ (unpaired t-test; $n = 9$ and 6/group respectively). **c** ejection fraction in mice administered $ScrA\beta_{42}$ or $A\beta_{42}$ (unpaired t-test; $n = 9$ and 10/group respectively). **d** fractional shortening in mice administered $ScrA\beta_{42}$ or $A\beta_{42}$ (unpaired t-test; $n = 9$ and 10/group respectively). **e** Expression of *Nppa* (Mann-Whitney test, U = 8), *Fap, Itga1, Rora* and *Fgfr1* in hearts of mice administered $ScrA\beta_{42}$ or $A\beta_{42}$ ($n = 8$ and 7/group respectively). All data are mean ± SEM. Statistical tests are two-tailed. Source data are provided in the Source Data file.

Supplementary Fig. 3f). Together with our previous findings, these data suggest that circulating $A\beta_{42}$, but not $A\beta_{40}$, has deleterious effects on the heart.

An Aβ neutralising antibody prevents obesity-induced impairment of cardiac relaxation

Having established that $A\beta_{42}$ release from adipose tissue is increased in obesity and that raising systemic concentrations of $A\beta_{42}$ negatively impacts cardiac metabolism and function, we next sought to determine whether $A\beta_{42}$ impairs cardiac relaxation in obesity, which is the initial defect in cardiac function that ultimately leads to heart failure[30]. We and others have previously established that deletion of *App* or components of the APP proteolytic machinery in mice increases energy expenditure and confers resistance to obesity[31,32]. Hence, these genetic models cannot be used to assess the role of $A\beta_{42}$ on cardiac function in obesity. Instead, the mouse-specific Aβ neutralising antibody 3D6 was employed to address this question. The binding of 3D6 to $A\beta_{42}$ prevents $A\beta_{42}$ interacting with receptors and the cellular internalisation of $A\beta_{42}$[33]. The humanised version of 3D6, bapineuzumab, reached phase III trials for AD[34]. Although it had excellent target engagement and an acceptable safety profile, it failed to produce meaningful improvements in cognition in AD patients[34]. Cardiovascular conditions were exclusion criteria for this and other AD trials, meaning that data on any potential cardiovascular effects are not available. Therefore, to determine whether $A\beta_{42}$ mediates the adverse effects of obesity on cardiac function, mice were fed a high-fat diet and were simultaneously administered 3D6 or a control antibody (0.75 mg/kg, i.p. once weekly) for a period of 4 months. Cardiac function and morphology were assessed by echocardiography at the beginning and conclusion of the experiment (Fig. 4a, Supplementary Fig. 4a). The initiating event in the development of obesity-induced cardiac dysfunction and eventual heart failure is impaired cardiac relaxation, which is characterised by increased deceleration time[35–37]. We have previously observed impairments in deceleration time in this model between 3-4 months of high-fat feeding[38]. Consistent with previous studies[39], 3D6 administration did not reduce total plasma $A\beta_{42}$ concentration (Fig. 4b) but did reduce the plasma concentration of free $A\beta_{42}$ that was unbound by antibodies (Fig. 4c). Administration of 3D6 had no effect on body weight (Fig. 4d), body composition or systemic metabolism (Supplementary Fig. 4b–f). In mice administered control antibody, deceleration time increased over the course of the high-fat feeding period (Fig. 4e). In contrast, deceleration time was not increased in mice administered 3D6 (Fig. 4e). The same result was observed when deceleration time was normalised as a percentage of the cardiac cycle (Supplementary Fig. 4g). Although initial estimated LV mass was not matched (but was not statistically different) between groups, LV mass was increased throughout the study in mice administered control antibody but was unchanged in mice administered 3D6 (Fig. 4f). A similar finding in left ventricular posterior wall thickness at diastole (LVPWd; Supplementary Table 3), an alternate index of LV mass[40], was observed. These data suggest that systemic $A\beta_{42}$ contributes to the obesity-induced impairment in cardiac relaxation and increase in LV mass.

An Aβ neutralising antibody prevents further impairment of cardiac relaxation in established obesity

The finding that $A\beta_{42}$ antagonism prevents obesity-induced impairment of cardiac relaxation raises the possibility that targeting $A\beta_{42}$ could be an effective treatment for established obesity-induced cardiac dysfunction. To test this hypothesis, mice were fed either standard chow or a high fat diet for 4 months and were administered 3D6 or control antibodies for the final 4 weeks of the experiment. Echocardiography to assess cardiac function and morphology was performed at the beginning of the experiment (baseline), prior to antibody treatment (pre-treatment) and at the conclusion of the study (post-treatment; Fig. 5a, Supplementary Fig 5a). Mice fed a high-fat diet had increased body weight (Fig. 5b), fat mass and fasting plasma insulin compared with chow-fed mice; however, 3D6 administration had no effect on these parameters (Supplementary Fig. 5b–e). There was no change in deceleration time in chow fed mice administered control antibody throughout the experiment (Fig. 5c).

https://doi.org/10.1038/s41467-023-44520-4

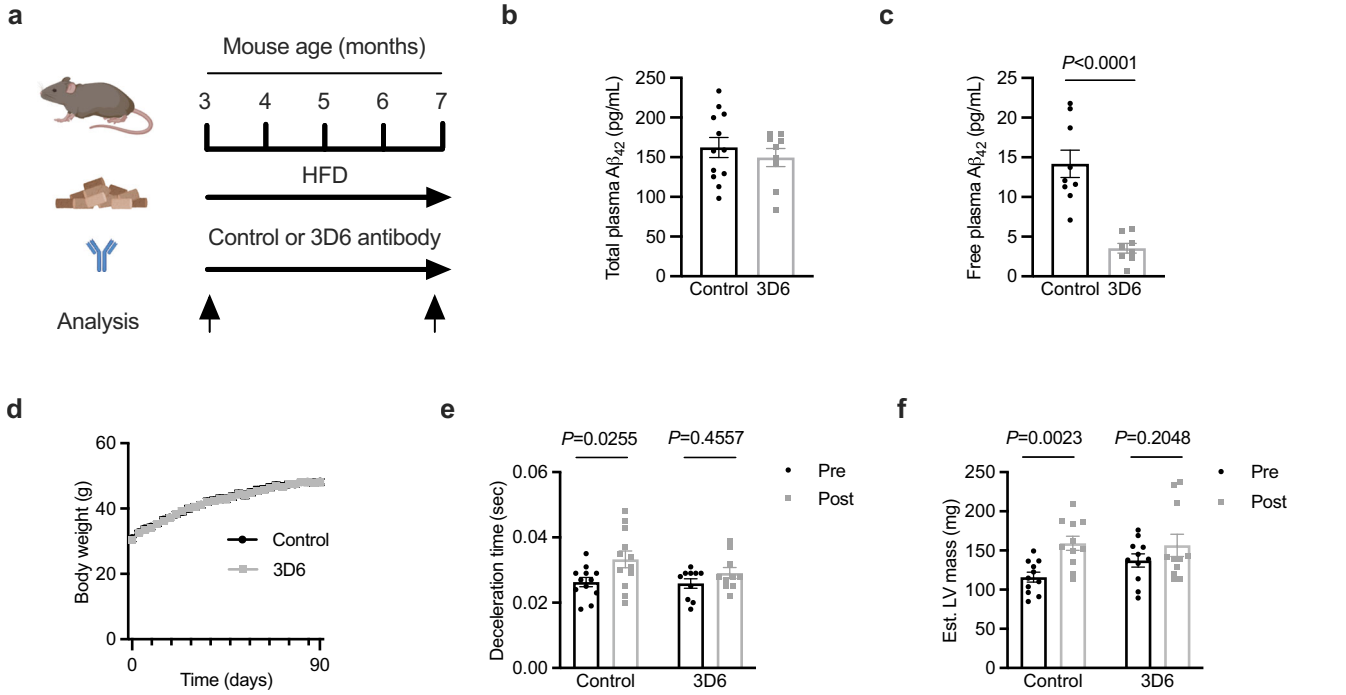

Fig. 4 | An Aβ$_{42}$ neutralising antibody prevents obesity-induced impairment of cardiac relaxation. a schematic of experiment where mice fed a high fat diet (HFD) for 4 months and were simultaneously administered a control antibody or an Aβ$_{42}$ neutralising antibody (3D6) once weekly. Analysis of cardiac function and morphology was performed at the beginning and end of the experiment. **b** total ($n = 12$ and 9/group respectively), and; **c**, free ($n = 9$ and 8/group respectively) Aβ$_{42}$ in plasma of mice administered control or 3D6 antibodies (unpaired t-test). **d** body weight of mice administered control or 3D6 antibodies ($n = 12$/group). **e** deceleration time in mice prior to and after 4 months of high-fat feeding and antibody administration (two-way repeated measures ANOVA (time $P = 0.0140$, $F(1,20) = 7.257$) and Sidak's multiple comparisons test P.adjusted; $n = 12$ and 10/group respectively). **f** estimated left ventricle (LV) mass in mice prior to and after 4 months of high-fat feeding and antibody administration (two-way repeated measures ANOVA (time $P = 0.0010$, $F(1,20) = 14.93$) and Sidak's multiple comparisons test P.adjusted; $n = 11$/group). All data are mean ± SEM. Statistical tests are two-tailed. Source data are provided in the Source Data file. Elements of **a** are created with BioRender.com.

Mice fed high fat diet and administered control antibody had an increase in deceleration time from baseline to pre-treatment, which increased further from pre-treatment to post-treatment (Fig. 5c). Mice fed high fat diet and administered 3D6 antibody had an increase in deceleration time from baseline to pre-treatment, however unlike mice administered control antibody, there was no further increase in deceleration time from pre-treatment to post-treatment (Fig. 5c). These findings were consistent when deceleration time was expressed as a percentage of the cardiac cycle (Supplementary Fig. 5f). Short term administration of 3D6 in established obesity did not alter any index of LV mass (Supplementary Table 4) but tended to increase cardiac glucose clearance (Fig. 5d and Supplementary Fig. 5g) and normalised cardiac TG concentrations (Fig. 5e). These data suggest that Aβ$_{42}$ antagonism halts further deterioration of cardiac relaxation in established obesity.

Aβ$_{42}$ reduces mitochondrial transcriptional programs and accumulates in cardiac mitochondria in obesity

In the context of AD, Aβ$_{42}$ has highly complex cellular effects through a myriad of mechanisms depending on the target cell type and its aggregation state[41]. To gain unbiased insights into the deleterious effects that Aβ$_{42}$ has on the heart, a multidimensional transcriptomic approach was employed. The transcriptomic profile of hearts obtained in Aβ$_{42}$ administration studies (Fig. 2a) were compared with the profile of hearts obtained in the 3D6 administration study (Fig. 4a) and pathways reciprocally regulated were identified using MITCH[42]. It was reasoned that reciprocally regulated pathways from these experiments represent geneset changes that are fundamental to the effects of Aβ$_{42}$ on the heart. Global gene expression across experiments was evenly distributed (Supplementary Fig. 6a and b). Multi-contrast enrichment analysis identified the TCA cycle, pyruvate metabolism and mitochondrial biogenesis pathways with the largest effect sizes that were reduced by Aβ$_{42}$ administration and increased by 3D6 administration (Fig. 6a and Supplementary Table 5). These pathways are dysregulated in obesity-induced cardiac dysfunction and have been linked with disrupted energetics that impair cardiac relaxation[24,43–45]. The transcriptional reprogramming of the TCA cycle included altered regulation of genes encoding TCA cycle enzymes (Fig. 6b), while transcriptional regulation of pyruvate metabolism included subunits of pyruvate dehydrogenase (PDH) and PDH kinases (PDKs; Fig. 6c). Regulated genes in the mitochondrial biogenesis pathway were mainly of nuclear transcription factors controlling the mitochondrial biogenesis process (Fig. 6d). Interestingly, several receptor pathways were increased by Aβ$_{42}$ administration and reduced by 3D6 administration (Fig. 6a and Supplementary Table 5). The widespread transcriptional reprogramming of mitochondrial pathways likely indicates a secondary response to the effects of Aβ$_{42}$ on mitochondria. Aβ$_{42}$ can be taken up by mitochondria, where it can impact numerous aspects of mitochondrial biology[15,46,47]. To examine whether Aβ$_{42}$ accumulates in mitochondria of the heart in obesity, enriched mitochondrial fractions were isolated from control and obese mice (Fig. 6e). Cardiac mitochondria from obese mice were found to have elevated concentrations of Aβ$_{42}$ (Fig. 6f). Interestingly, mitochondrial Aβ$_{42}$ was also increased in the skeletal muscle of obese mice, but not in adipose tissue or in the liver (Supplementary Fig. 6c), suggesting that striated muscle specifically has a propensity to accumulate Aβ$_{42}$ in obesity. Furthermore, Aβ$_{42}$ concentrations were reduced in cardiac mitochondria in obese mice that were administered 3D6 antibodies (Fig.6g), consistent with reports that this antibody enhances tissue Aβ clearance[48].

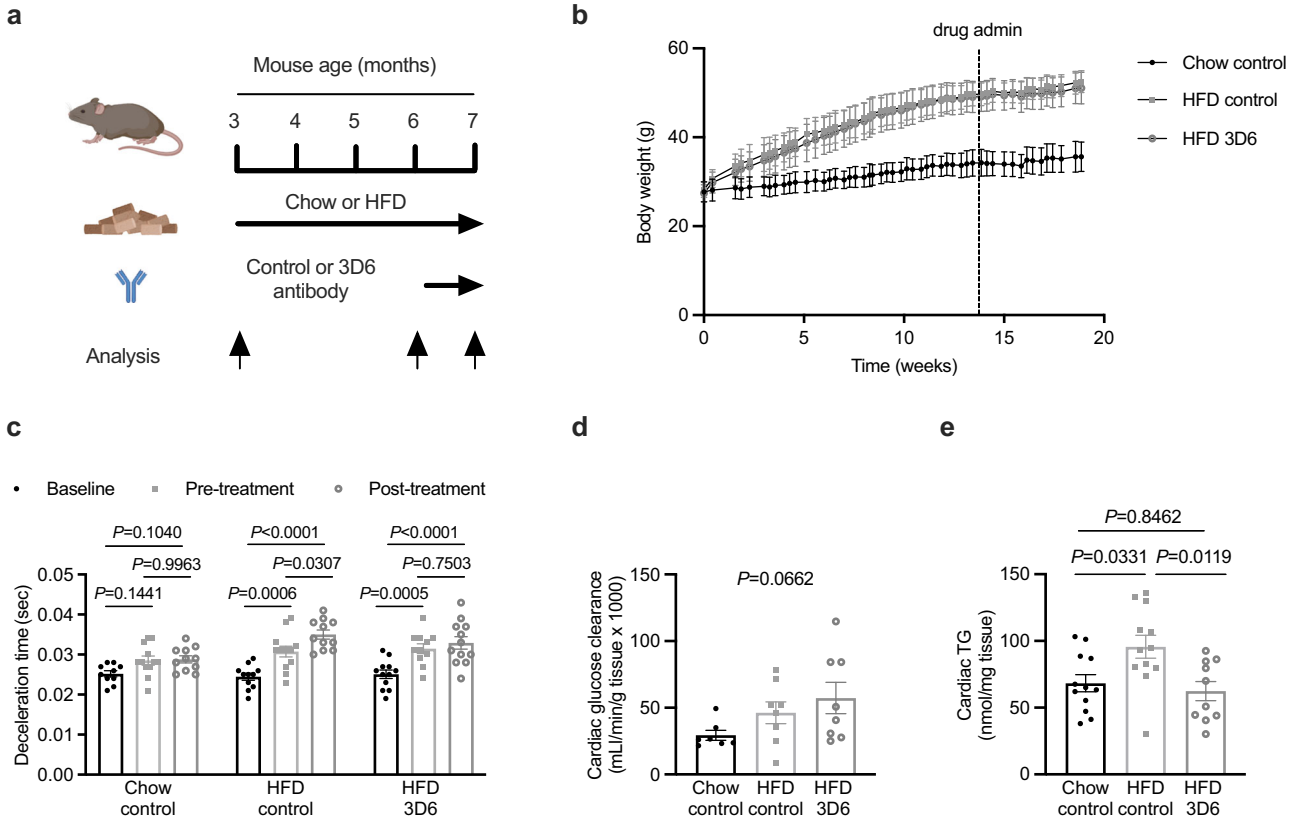

Fig. 5 | An Aβ$_{42}$ neutralising antibody prevents further impairment of cardiac relaxation in established obesity. a schematic of experiment where mice fed either chow or a high-fat diet (HFD) for 4 months and were administered a control antibody or an Aβ$_{42}$ neutralising antibody (3D6) once weekly in the final month of the diet period. Analysis of cardiac function and morphology was performed at the beginning and of the experiment (baseline), prior to the treatment period (pre-treatment) and at the end of the treatment period (post-treatment). **b** body weight over time in mice fed regular chow or HFD and administered control or 3D6 antibodies ($n = 12$/group). **c** deceleration time in mice at Baseline, pre-treatment and post-treatment after 4 months of chow or high fat feeding and antibody administration (mixed-effects model (time $P < 0.0001$, $F(2,93) = 31.56$; treatment $P = 0.0151$, $F(2,93) = 4.390$) and Sidak's multiple comparisons test P.adjusted; $n = 12$/group). **d** cardiac glucose clearance ($n = 8$, 9 and 9/group respectively), and; **e** cardiac triglycerides (TG; One-way ANOVA, $P = 0.0082$, $F(2,31) = 5.624$; $n = 12$, 12 and 10/group respectively) in mice fed regular chow and administered control antibody, or mice fed a high fat diet (HFD) and administered control or 3D6 antibodies. All data are mean ± SEM. Statistical tests are two-tailed. Source data are provided in the Source Data file. Elements of **a** are created with BioRender.com.

Aβ$_{42}$ inhibits mitochondrial complex I in cardiomyocytes

Identification of the mitochondrial target of Aβ$_{42}$ was further explored. Upon cellular uptake and mitochondrial import, Aβ$_{42}$ is known to physically interact with and inhibit complex I of the respiratory chain[49]. Complex I is a candidate target for Aβ$_{42}$ in the context of obesity, which is characterised by reduced complex I function in the heart[43,50,51]. As gene expression profiling suggested that the effects of Aβ$_{42}$ on mitochondria were specific for cardiomyocytes (Fig. 2l), a primary neonatal ventricular cardiomyocyte model system was used to examine whether Aβ$_{42}$ inhibits complex I in cardiomyocytes. Exposure of cardiomyocytes to increasing concentrations of Aβ$_{42}$ for 48hrs reduced cardiomyocyte oxygen consumption rate (OCR; Fig. 7a) as well as maximal respiratory capacity (Fig. 7b). This was not explained by a loss of cell viability (Supplementary Fig. 7a) and indicate that Aβ$_{42}$ has direct effects on cardiomyocytes. Exposure of Aβ$_{42}$ to FAO hepatocytes did not have any effect on basal respiration (Supplementary Fig. 7b), suggesting cell type-specific effects of Aβ$_{42}$. Sensitivity to the complex I inhibitor rotenone (Fig. 7c), but not the unrelated ATP synthase inhibitor oligomycin (Supplementary Fig 7c), was altered following exposure of cardiomyocytes to Aβ$_{42}$ and was associated with reduced complex I-mediated respiration (Fig. 7d). To dissect whether the effects of Aβ$_{42}$ on complex I could be explained by the reduction in respiratory capacity, complex I-mediated respiration was expressed relative to maximal respiratory capacity and was reduced by exposure to Aβ$_{42}$ (Fig. 7e). This provides further evidence that Aβ$_{42}$ inhibits complex I of the respiratory chain as well as reducing mitochondrial capacity in cardiomyocytes, both of which have been observed in heart failure[43,51–53]. These findings suggest that systemic Aβ$_{42}$ is internalised and taken up by mitochondria in cardiomyocytes, where it can impair mitochondrial respiratory function.

Discussion

Our findings have revealed an unexpected role for Aβ$_{42}$ in the aetiology of obesity-induced cardiac dysfunction (Fig. 7f). Factors such as increased adiposity, myocardial lipid accumulation and cardiomyocyte mitochondrial dysfunction have all been implicated in the development of diastolic dysfunction in obesity. Data generated in the present study indicates that Aβ$_{42}$ is a unifying link between all of these factors and is supported by a recent study, published while the current manuscript was in preparation, proving the association between circulating Aβ and heart failure in the general population[54]. Our data advances our understanding of the impact of obesity on the heart and identify an actionable target for therapeutic intervention in obesity-induced heart failure.

In humans, both total fat mass and visceral fat mass are associated with impaired myocardial energetics and diastolic dysfunction[24]. Although increased free fatty acid availability that leads to myocardial lipid accumulation is one potential mechanism describing this association, diastolic dysfunction in humans occurs with moderate visceral adiposity before the appearance of myocardial lipid accumulation[24].

https://doi.org/10.1038/s41467-023-44520-4

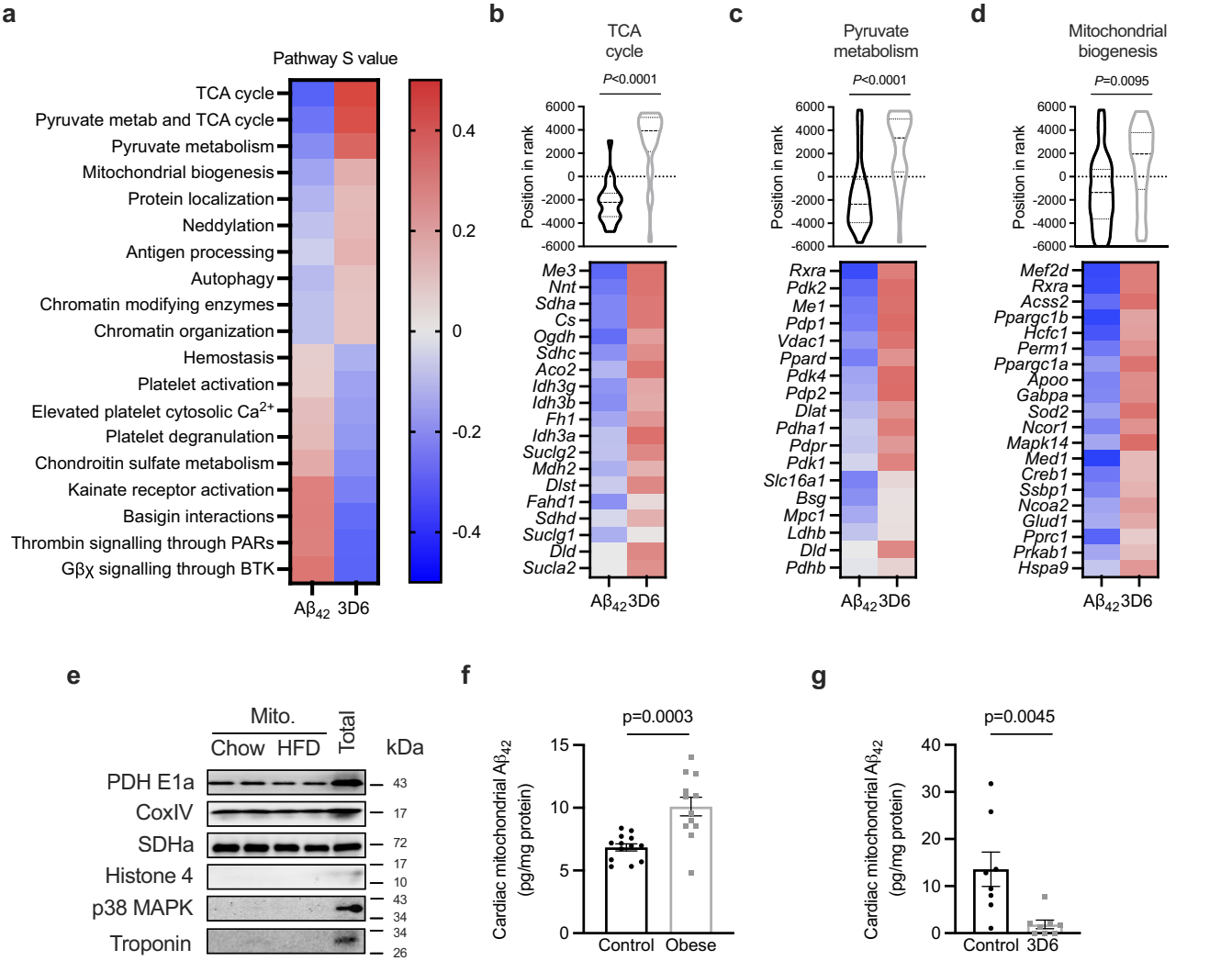

Fig. 6 | $A\beta_{42}$ impairs mitochondrial transcriptional programs and accumulates in cardiac mitochondria in obesity. a heat map of Reactome pathways reciprocally regulated in the hearts of mice from $A\beta_{42}$ (Fig. 2a) and 3D6 (Fig. 3a) administration studies, determined by MITCH analysis from bulk RNA-seq data. **b** TCA cycle pathway rank (*P*.adjusted MANOVA test) and heat map of TCA cycle genes in the hearts of mice from $A\beta_{42}$ and 3D6 administration studies. **c** pyruvate metabolism pathway rank (*P*.adjusted MANOVA test) and heat map of pyruvate metabolism genes in the hearts of mice from $A\beta_{42}$ and 3D6 administration studies. **d** mitochondrial biogenesis pathway rank (*P*.adjusted MANOVA test) and heat map of mitochondrial biogenesis genes in the hearts of mice from $A\beta_{42}$ and 3D6 administration studies. **e** characterisation of enriched mitochondrial fractions from hearts of chow or high fat diet (HFD)-fed mice. **f** $A\beta_{42}$ in mitochondrial fractions isolated from hearts of chow or HFD-fed mice (unpaired t-test; $n = 13$ and 12/group respectively). **g** $A\beta_{42}$ in mitochondrial fractions isolated from hearts of mice fed HFD and administered control or 3D6 antibodies (Fig. 3a; unpaired t-test; $n = 8$/group). All data are mean ± SEM. Statistical tests are two-tailed. Source data are provided in the Source Data file.

One interpretation of these data is that factors released by adipose tissue other than fatty acids, such as $A\beta_{42}$, are more important contributors to obesity-induced diastolic dysfunction. While adipose tissue could be a major source of $A\beta_{42}$ in obesity, the exact cell types involved remain obscure. In addition to adipocytes, vascular endothelial cells and immune cells, which infiltrate adipose tissue in obesity, are all candidate cell types that express high levels of APP and the APP processing machinery and could release Aβ peptides, particularly under metabolic conditions associated with obesity[55–57].

Increasing systemic $A\beta_{42}$ reprogrammed cardiac glucose metabolism, including reduced glucose clearance and increasing glucose incorporation into lipids. It is well established that impairments in cardiac glucose metabolism are associated with impairments in cardiac function[58–61]. Consistent with these findings, administration of $A\beta_{42}$ to normal mice resulted in wide-ranging defects in both diastolic and systolic function. However, the early stages of obesity, in both mice and humans, are generally not associated with systolic dysfunction, despite elevated circulating $A\beta_{42}$. This discrepancy is likely due to whole-body metabolic and hormonal alterations in obesity that minimise the impact of $A\beta_{42}$ on the heart, restricting its effects to relaxation defects that manifest as diastolic dysfunction.

While preparing this manuscript, it was reported that plasma concentrations of both $A\beta_{42}$ and $A\beta_{40}$ are associated with heart failure in the general population, particularly in males[54]. While the association was stronger for $A\beta_{40}$, this could be due to the greater propensity for $A\beta_{42}$ to leave the circulation and accumulate in vascular beds and in tissues[62]. Indeed, in our administration studies, the delivery of equal amounts of $A\beta_{40}$ and $A\beta_{42}$ resulted in a greater plasma excursion of $A\beta_{40}$ (Fig. 2b and Supplementary Fig. 3b). Our findings are also consistent with associative observations in patients with AD, whereby $A\beta_{42}$ accumulates in the heart and is associated with diastolic dysfunction[63].

The accumulation of $A\beta_{42}$ in cardiac mitochondria and the $A\beta_{42}$-mediated reduction in complex I-associated respiration in cardiomyocytes phenocopies aspects of $A\beta_{42}$ biology in AD. A recent study

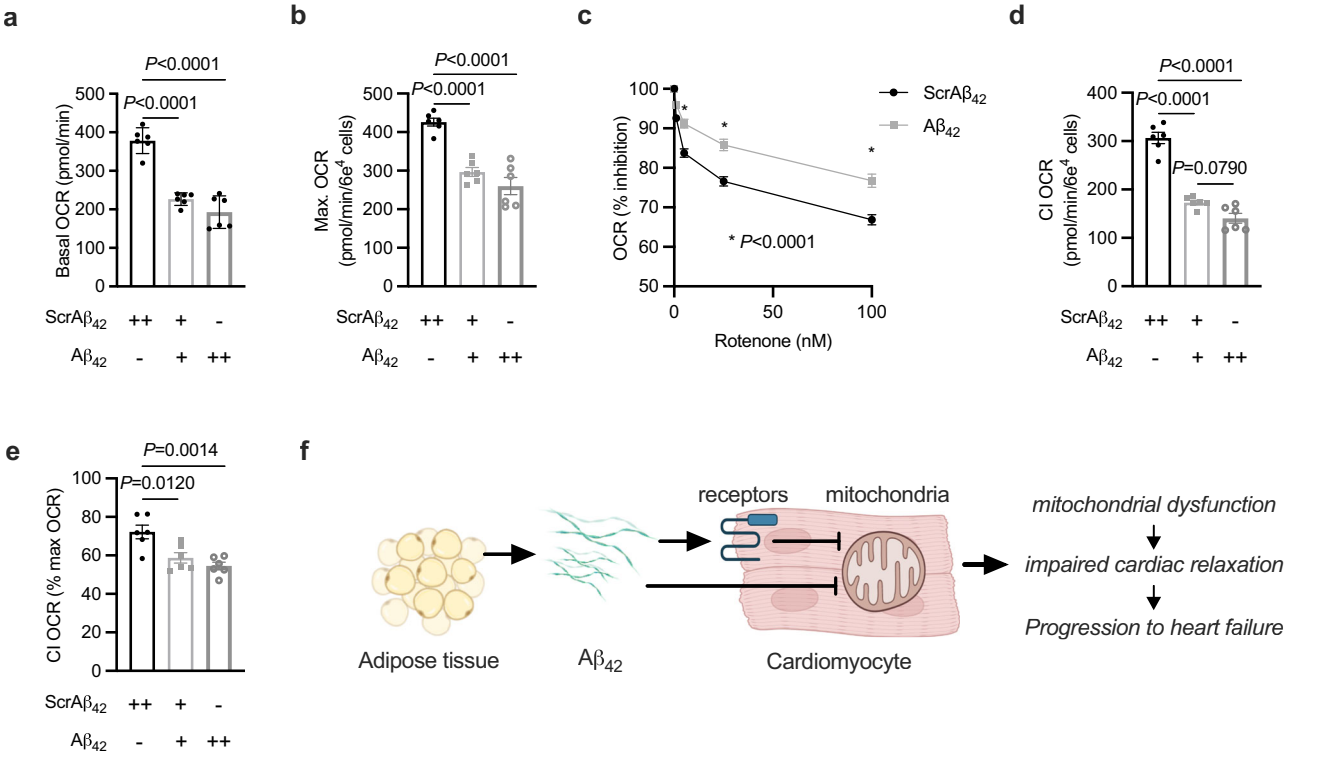

Fig. 7 | $A\beta_{42}$ inhibits mitochondrial complex I in cardiomyocytes. a Basal oxygen consumption rate (OCR) in primary mouse neonatal cardiomyocytes (NVCM) exposed to Scr$A\beta_{42}$ or $A\beta_{42}$ (Scr$A\beta_{42}$ at 300 (++), 100 (+) and 0pM (−) and co-incubated with $A\beta_{42}$ at 0 (−), 200 (+) and 300pM (++) for 48 hrs (one-way ANOVA ($P < 0.0001$; $F(2,15) = 53.5$) with Sidak's repeated measures test *P*.adjusted; $n = 6$ biological replicates/group). **b** maximal OCR in primary NVCM exposed to Scr$A\beta_{42}$ or $A\beta_{42}$ for 48 hrs (one-way ANOVA ($P = 0.0001$; $F(2,15) = 31.2$) with Sidak's repeated measures test *P*.adjusted; $n = 6$ biological replicates/group). **c** inhibition of respiration in response to increasing concentrations of rotenone in primary NVCM exposed to Scr$A\beta_{42}$ or $A\beta_{42}$ for 48 hrs (multiple t-tests *P*.adjusted; $n = 5$ biological replicates/group). **d** absolute complex I (CI) OCR in primary NVCM exposed to Scr$A\beta_{42}$ or $A\beta_{42}$ for 48 hrs (one-way ANOVA ($P < 0.0001$; $F(2,15) = 88.4$) with Sidak's repeated measures test *P*.adjusted; $n = 6$ biological replicates/group). **e** complex I (CI) OCR as a percentage of total respiratory capacity in primary NVCM exposed to Scr$A\beta_{42}$ or $A\beta_{42}$ for 48 hrs (one-way ANOVA ($P < 0.0012$; $F(2,15) = 10.8$) with Sidak's repeated measures test *P*.adjusted; $n = 6$ biological replicates/group). All data are mean ± SEM. All statistical tests are two-tailed. Source data are provided in the Source Data file. **f** schematic of proposed model whereby adipose tissue release of $A\beta_{42}$ is increased in obesity resulting in higher circulating levels of $A\beta_{42}$. Increased circulating $A\beta_{42}$ inhibits cardiomyocyte mitochondrial ATP production and causes diastolic dysfunction, which starts the progression towards heart failure. The effects of $A\beta_{42}$ on cardiomyocytes could be mediated through receptor-mediated signalling, receptor-mediated internalisation, or direct internalisation. **e** was created with BioRender.com.

suggests that other aspects of mitochondrial function are also impacted by $A\beta_{42}$ in cardiomyocytes[64]. The extent to which the effects of $A\beta_{42}$ on complex I account for the metabolic and contractile impairments that occur in cardiomyocytes in obesity in vivo remains to be determined. However, we hypothesise that complex I is a major site of metabolic impairment in the heart in obesity and could explain the defects in glucose oxidation that are observed in heart failure. Complete oxidation of glucose primarily generates NADH as the intermediate electron carrier, which is oxidise by complex I of the respiratory chain. In contrast, beta-oxidation of fatty acids generates substantial $FADH_2$ that is oxidised by complex II of the respiratory chain and complex I inhibition increases fatty acid oxidation in a variety of cell types[65–67]. A limitation of the current study is that the effect of $A\beta_{42}$ on mitochondria was examined in neonatal cardiomyocytes. This model was used rather than adult cardiomyocytes, as the latter are prone to extensive cell death and alterations in cellular identity in the first 24-48 hr of culturing[68], which could confound the effects of $A\beta_{42}$. It is well established that neonatal cardiomyocytes oxidise proportionally more glucose and less fatty acids than adult cardiomyocytes[69]. Therefore, further studies examining how $A\beta_{42}$ impacts mitochondrial substrate utilisation are warranted. As adult primary cardiomyocytes quickly de-differentiate and reprogram mitochondrial capacity accordingly[70], sophisticated studies in vivo will be required to properly dissect the metabolic effects of $A\beta_{42}$ on cardiomyocytes and the heart.

This study supports the idea that therapies originally designed for AD that reduce or antagonise $A\beta_{42}$ could be repurposed to treat and/or prevent obesity-induced heart failure[71], particularly those with HFpEF, for which treatment options are limited[25]. This is an urgent unmet need as this patient group has a 5-year mortality rate of up to 75% and currently affects up to 8% of people in certain populations[30]. Furthermore, the prevalence of HFpEF is predicted to rise in parallel with rising rates of obesity[30]. A suite of biologics and small molecules has been developed for AD that antagonise or reduce $A\beta_{42}$, many with well-established safety and tolerability profiles in humans. These diverse therapies with distinct mechanisms of action could therefore be rapidly assessed as new treatments for heart failure in obesity.

In conclusion, this study has identified a link between adiposity, $A\beta_{42}$ release from adipose tissue and impairments in cardiac metabolism and function. The data generated highlight mechanistic similarities in the development of obesity-induced cardiac dysfunction and AD and support the idea that repurposing drugs originally developed for AD could be an approach to treat and manage heart failure.

Methods

Animal studies

Male C57BL6J mice were used for all mouse experiments and were obtained from the Animal Resources Centre (Perth, WA, Australia) and were group housed with four to five mice per cage with a 12 h light/dark cycle at 22 °C with humidity 20–60%. Animals had ad libitum

access to food (12.8 kJ/g, 6% fat, 20% protein; Barastoc Mouse Maintenance Cube, Ridley AgriProducts) and water. All procedures involving animals were approved by The Deakin University Animal Welfare Committee (A58-2010, G07-2013, G15-2017 and G08-2020), which is subject to the Australian Code for the Responsible Conduct of Research.

High-fat feeding. At 12 weeks of age, mice were randomly assigned to regular chow or high-fat diet (HFD; 43% digestible energy from fat, 20% from sucrose; SF04-001 Specialty Feeds). Throughout the diet period, mice were weighed weekly. After three months of the diet period, mice underwent body composition assessment using EchoMRI. Two days later, mice were fasted for 5 hrs before being humanely killed by cervical dislocation. Epididymal and inguinal adipose tissues were carefully excised and weighed and were either immediately frozen and stored at −80 °C for later analysis or were used for ex vivo adipose explant experiments.

Aβ peptide administration. Lyophilised recombinant $Aβ_{42}$ (#AG912, Millipore) and scrambled control peptide ($ScrAβ_{42}$; #AG916, Millipore) were resuspended in 1% NH_4OH and aliquoted at 200 ng/ml in H_2O and stored at −80 °C for no longer than 4 weeks. Peptide administration began when mice were 10-12 weeks of age and involved a daily i.p. injection of 1µg of peptide. Throughout the peptide administration period, body weight was measured daily and food intake was measured twice weekly, and body composition was measured weekly by EchoMRI. After two weeks, plasma $Aβ_{42}$ was determined from samples collected 5 hr after recombinant $ScrAβ_{42}$ or $Aβ_{42}$ administration. After 3 weeks, an insulin tolerance test (ITT; i.p. 0.75U/kg) was performed following a 5 hr fast and 5 hr after peptide administration. Blood glucose was measured at baseline and after 20, 40, 60, 90 and 120 min after glucose administration. One week later, a glucose tolerance test (GTT; i.p 2 g/kg with 5µCi ^{3}H-2-deoxyglucose and 5µCi ^{14}C-glucose) was performed after a 5 hr fast and 5 hr after peptide administration. Blood glucose was measured at baseline and after 15, 30, 45, 60 and 90 min after glucose administration. Plasma was obtained at 0, 15, 30, 60 and 90 min for insulin determination and the measurement of tracer-specific activity. Mice were humanely killed by cervical dislocation immediately after the GTT. Blood was collected for plasma and tissues were dissected, rapidly frozen and stored at −80 °C for later analysis. Another cohort of mice were administered $ScrAβ_{42}$ or $Aβ_{42}$ for four weeks, as described above. After four weeks of peptide administration, mice were anaesthetised by isoflurane inhalation before undergoing echocardiography. Two days later, mice were humanely killed by cervical dislocation and blood was obtained for plasma and tissues were dissected, rapidly frozen and stored at −80 °C for later analysis. Another cohort of mice were administered $ScrAβ_{40}$ or $Aβ_{40}$ (Millipore) for four weeks, as described above. After four weeks of peptide administration, mice were anaesthetised by isoflurane inhalation before undergoing echocardiography. Two days later, mice were humanely killed by cervical dislocation and blood was obtained for plasma and tissues were dissected, rapidly frozen and stored at −80 °C for later analysis.

3D6 administration. For the 3D6 prevention study, 12-week-old mice were assessed for baseline cardiac structure and function by echocardiography and were assigned to one of two groups such that deceleration time was matched. One week later, mice were fed HFD (as described above) and then received control antibody (IgG2a isotype antibody, #BE-0085 BioXCell) or 3D6 antibody (#TAB-0809CLV, Creative Biolabs) weekly via i.p. injection (0.75 mg/kg). Body weight was measured twice per week, while body composition was measured every two weeks throughout the study. After 10 weeks of high-fat feeding, mice underwent an ITT and then a GTT after 11 weeks of high-fat feeding. After 12 weeks of high-fat feeding mice underwent echocardiography and two weeks later were humanely killed by cervical dislocation following a 5 hr fast. Blood was collected for plasma and tissues were dissected, rapidly frozen and stored at −80 °C for later analysis. In the 3D6 reversal study, 12-week-old mice were assessed for baseline cardiac structure and function by echocardiography and were assigned to one of three groups such that deceleration time was matched. One week later, one group of mice remained on standard chow, while the other two groups were fed a high-fat diet. Body weight was measured twice per week throughout the study. After 13 weeks of high-fat feeding, mice underwent echocardiography for pre-treatment assessment of cardiac function and morphology. Mice were then administered control antibody or 3D6 antibody weekly via i.p. injection (0.75 mg/kg) for the remainder of the study. Four weeks later, mice underwent post-treatment assessment of cardiac function and morphology, followed by assessment of body composition by EchoMRI two days later. One week later, mice were humanely killed by cervical dislocation following a 5 h fast. Blood was collected for plasma and tissues were dissected, rapidly frozen and stored at −80 °C for later analysis.

Echocardiography. Echocardiography was performed using a Phillips HD15 diagnostic ultrasound system with 15 MHz linear-array transducer[38,72,73]. In line with published recommendations[74], depth of anaesthesia was modulated to maintain heart rate between 400 and 650 bpm. Images were not quantified when heart rate was ≤ 350 bpm. Transmitral Doppler imaging was used to assess LV filling velocity and deceleration time was determined from the slope of the E-wave. Only E-waves where there was sufficient separation from the A-wave to allow slope determination were quantified. Aortic valve Doppler imaging was used to assess aortic flow and ejection times. Ejection fraction and fractional shortening (FS) were derived from M-Mode measurements as indicators of LV systolic and contractile function and chamber morphology was also determined from M-mode measures. Echo images were analysed using the HD15 system in a blinded manner. The average value of each index from 2-4 cardiac cycles was used.

Adipose tissue explants

Prior to the ex vivo incubation protocol, all consumables such as 12-well plates, tips, and tubes were blocked in 5% bovine serum albumin (BSA) to minimise binding of $Aβ_{42}$ to plasticware[75]. Tests with recombinant $Aβ_{42}$ revealed recovery of ~95% of $Aβ_{42}$ using this method. Upon collection of inguinal adipose tissue samples, four ~10–15 mg tissue portions were isolated and each of them was placed in a well with 500 uL of DMEM media supplemented with 10% BSA. Three samples were incubated in vehicle (0.1% DMSO), while one incubated in 10µM Brefeldin A. Each tissue was individually weighed, the starting time of the incubation recorded, and the plate was placed at 37 °C in 10% CO_2 for 24 h. Following the 24 h period, both media and the tissue were rapidly collected, and subsequently snap-frozen, for further analyses. High-sensitivity ELISA kits were used to quantify $Aβ_{40}$ (#294-62501 human/rat/mouse, FUJIFILM Wako) and $Aβ_{42}$ (#292-64501 human/rat/mouse high sensitivity, FUJIFILM Wako) and the protocol was followed as per the manufacturer's protocol. In brief, samples were brought to room temperature, vortexed, and 100 µl of sample was placed in each well, together with the respective internal controls for each plate. Each plate was then sealed and refrigerated overnight. Following this, the solutions were discarded, and each well was washed 5 times before addition of 100 µl of HRP-conjugated antibody. Following 1 hour of incubation, the solution was discarded and the washing step was repeated, with subsequent addition of 100 µl TMB solution to initiate the HRP reaction at room temperature in the dark. Following 30 minutes, 100 µl of Stop-solution was added to terminate the reaction and the absorbance (at 450 nm) was subsequently measured to determine the protein levels.

Glucose clearance and fate

The LV of the heart, quadriceps skeletal muscle and epididymal adipose tissue (15-25 mg) were used to determine 2-^{2}H-deoxyglucose clearance as we have previously described[73]. To determine 1-^{14}C-glucose incorporation into glycogen, ~10-15 mg of LV tissue was digested in 1 M KOH at 70 °C for 20 min and glycogen was precipitated with saturated Na_2SO_4, washed twice with 95% ethanol and resuspended in acetate buffer (0.84% sodium acetate, 0.46% acetic acid, pH 4.75) containing 0.3 mg/mL amyloglucosidase (Sigma). Glycogen was allowed to digest overnight at 37 °C before being assayed for glucose content using the glucose oxidase method[76]. Digested glycogen was also assessed for ^{14}C-glucose incorporation by scintillation counting. To determine 1-^{14}C glucose incorporation into lipids, 5–10 mg of LV tissue was homogenised in chloroform/methanol (2:1) and mixed overnight at room temperature. Organic and inorganic phases were separated by addition of 0.6% NaCl and the lower organic phase was collected and evaporated under N_2 at 45 °C. The dried extract was resuspended in absolute ethanol and TG content was assayed using TG GPO-PAP reagent (Roche) and ^{14}C-glucose incorporation by scintillation counting.

Gene expression and analysis

Bulk RNA was isolated from LV tissue by homogenisation using a handheld homogeniser in Trizol and RNA was isolated using RNeasy kits (Qiagen), according to manufacturer's instructions. Sequencing libraries were generated from 0.5 μg of total RNA using TruSeq Stranded Total RNA preparation kit (Illumina) as per manufacturer's instructions. Transcriptome-wide mRNA levels were measured using the NovaSeq 6000 Sequencing System (Illumina). Sequence Fastq files underwent quality trimming and mapping to the mouse reference transcriptome with Salmon. The reference transcriptome sequence was obtained from Gencode (version vM24). Counts were read into R (version 4.0.2)[77]. Differential expression analysis was performed separately for two contrasts (Scr$A\beta_{42}$ vs. $A\beta_{42}$ and Control vs 3D6). Genes with fewer than 10 reads per sample on average were discarded. Differential analysis was performed with DESeq2 (version1.28.1). Multicontrast enrichment analysis was performed with mitch (version 1.0.6) using default settings, which implements an ANOVA on ranks approach[42]. Human Reactome pathways were downloaded (19th May 2020) and gene names were converted to mouse using Ensembl ortholog mapping. Gene sets with false discovery rate <0.05 were considered significant. Genesets that were significantly regulated in both contrasts were presented. The expression of *App, Bace1 and Psen1* were quantified in epididymal adipose tissue, quadriceps skeletal muscle and the liver of control and obese mice by real time RT-PCR using the following primer pairs (*App* Fwd CTTGCACGACTATGG CATGC, rev GTCATCCTCCTCTGCATCCG; *Bace1* Fwd GGAGCCCTT CTTTGACTCCC, rev CCCGTG TATAGCGAGTGGTC; *Psen1* Fwd TTCA AGAAAGCGTTGCCAGC, rev AGGGCTGCACA AGGTAATCC).

Plasma and biochemical analyses

BACE-1 activity was assessed using a fluorescent assay kit (Merck), while plasma glycerol and plasma HDL-C were determined using colorimetric kits (Sigma), all according to manufacturer's instructions. High-sensitivity ELISAs were used to measure plasma $A\beta_{40}$ and $A\beta_{42}$ (FUJIFILM Wako), as described above, and plasma insulin (ALPCO), according to manufacturer's instructions. Plasma TG concentration was assayed using TG GPO-PAP reagent (Roche) and plasma NEFA was determined using a colorimetric kit (FUJIFILM Wako). To quantify free plasma $A\beta_{42}$, 100μL of plasma was added to 150μL of 10 mM Tris pH 7.5 and incubated with protein G magnetic beads, for 2 hours at 4 °C on a rotating wheel, before being spun in a centrifuge at 5,000 g for 5 min at 4 °C. The supernatant was collected and 100 μL was used to quantify $A\beta_{42}$ using a high-sensitivity ELISA, as described above. Protein G beads were blocked with 0.2% BSA in 10 mM Tris pH 7.5 overnight at 4 °C on a rotating wheel prior to the assay.

Isolation of enriched mitochondrial fractions

Approximately 50 mg of left ventricular tissue was homogenised with a handheld homogeniser at low speed for two 10 sec bursts while on ice in 500μL of mitochondrial isolation buffer (70 mM sucrose, 220 mM mannitol, 5 mM KH_2PO_4, 5 mM $MgCl_2$, 2 mM HEPES, 1 mM EGTA, 0.2% BSA). The homogenate was spun in a centrifuge at 800 g for 10 min at 4 °C. The supernatant was collected and spun in a centrifuge at 12,000 g for 10 min at 4 °C. The resulting pellet was resuspended in lysis buffer (50 mM Tris pH 7.5, 1 mM EDTA, 1 mM EGTA, 10% glycerol, 1% triton X-100, 50 mM NaF, 5 mM $Na_4P_2O_7$, 1 mM Na_3VO_4, 1 mM DTT) and mitochondrial protein concentration was determined by the BCA method. Quantification of $A\beta_{42}$ was performed from 200μg of mitochondrial protein.

Western blotting

For western blotting, 10 μg of protein were denatured in SDS reducing buffer and incubated at 37 °C for 5 min before being subjected to SDS-PAGE[78]. Proteins were transferred onto polyvinylidine diflouride (PVDF) membranes, which were blocked in 1% bovine serum albumin in Tris-buffered saline and 0.05% Tween (TBST) for 1 hour at RT before being exposed to primary antibodies against pyruvate dehydrogenase (PDH) E1a subunit (Cell Signalling Technology #2784), cytochrome c oxidase subunit 4 (CoxIV; Cell Signalling Technology #4844), succinate dehydrogenase subunit A (SDHa; Cell Signalling Technology #11998), histone 4 (H4; Cell Signalling Technology #2592) p38 mitogen activate protein kinase (MAPK; Cell Signalling Technology #9212), troponin (Cell Signalling Technology #4002), amyloid beta (Moab2, Abcam ab126649) and α-tubulin (Sigma-Aldrich T6074). All antibodies were diluted in 1xTBST at a concentration of 1:1000. Membranes were washed in TBST and exposed to appropriate anti-species horseradish peroxidase (HRP) conjugated secondary antibodies for 1 hr at RT, before final washes. Protein bands were detected using ECL Chemiluminescent Substrate Reagent Kit (Invitrogen) and visualized on a Chemidoc XRS System and Analysis Software (Bio-Rad Laboratories).

Primary cardiomyocytes

Neonatal ventricular cardiomyocytes were isolated from mixed sex, two-day-old C57BL6J mice[79]. Cells were seeded into Seahorse V7 assay plates at 60,000 cells/well. Prior to assays, cells were exposed to $A\beta_{42}$ at 0, 200 and 300pM and co-incubated with Scr$A\beta_{42}$ at 300, 100 and 0pM, respectively, such that all cells were exposed to 300pM of total peptide for 48 hr, with media replenished every 24 hr. These supraphysiological $A\beta_{42}$ concentrations were used as we measured $A\beta_{42}$ levels in FBS containing media at ~20pM. Cells were washed and incubated in 600 μL assay running media (unbuffered DMEM, Invitrogen; supplemented with 25 mM glucose, 1 mM pyruvate, pH 7.4) in a non-CO_2 incubator at 37 °C for 1 h before commencing the assay. Mitochondrial function was analysed by performing three baseline oxygen consumption rate (OCR) measurements, before subsequent measurements following injections of oligomycin (1 mM final concentration), carbonyl cyanide-p-trifluoromethoxyphenylhydrazone (FCCP; 1 μM final concentration), rotenone (1 μM final concentration) and Antimycin A (1 μM final concentration). Each measurement cycle consisted of the following: 3 min mix, 3 min wait, 3 min measure. Basal OCR was calculated by subtracting the mean value of the OCR measurements following Antimycin A injection from the mean of the baseline measurements. Maximal OCR was calculated by subtracting the mean value of the OCR measurements following Antimycin A injection from the mean value of the OCR measurements following FCCP injection[80]. Complex I-mediated respiration was designated as the difference between basal and rotenone (1μM)-suppressed respiration, which was also normalised by the maximal respiratory rate under FCCP stimulated conditions to determine flux as a percentage of maximal capacity. Cell viability was assessed by measuring extracellular and intracellular lactate dehydrogenase (LDH) following

exposure of cardiomyocytes to 300pM of Scr$A\beta_{42}$ or $A\beta_{42}$ for 48 hrs. LDH was measured using the CytoTox 96® Non-Radioactive Cytotoxicity Assay kit (Promega) as per manufacturer's instructions. Viability was expressed as LDH in the media normalised to total LDH from the media and cell lysate[76].

Statistical analyses

All data are presented as mean ± SEM. Individual data points identified as greater than two standard deviations away from the mean were designated as outliers and removed. Data were assessed for normality using a Shapiro-Wilks test. Normally distributed data were analysed by independent samples t-test, one-way ANOVA, two-way ANOVA, two-way repeated measures ANOVA or mixed effects model, as described for statistically significant data in relevant figure legends. Data not normally distributed were analysed by Mann-Whitney test or Kruskal-Wallis test, as described for statistically significant data in relevant figure legends. All statistical analyses were performed using GraphPad Prism 9, with p values < 0.05 considered significant.

Reporting summary

Further information on research design is available in the Nature Portfolio Reporting Summary linked to this article.

Data availability

RNA-seq data generated in this study can be found at Gene Expression Omnibus, submission GSE213708. All other data generated during this study are provided in the Source Data file. No previously published datasets were used in this work. Source data are provided with this paper.

Code availability

Scripts used for differential gene expression, enrichment analysis and mitch, as well as specific instructions for how to reproduce our data, are provided at the following link (https://github.com/markziemann/2dpw4liam). Code is also accessible and citable at https://doi.org/10.5281/zenodo.10203716.

References

1. Gustafson, D., Rothenberg, E., Blennow, K., Steen, B. & Skoog, I. An 18-year follow-up of overweight and risk of Alzheimer disease. *Arch. Internal Med.* **163**, 1524–1528 (2003).
2. Stampfer, M. J. Cardiovascular disease and Alzheimer's disease: common links. *J. Internal Med.* **260**, 211–223 (2006).
3. Powell-Wiley, T. M. et al. Obesity and Cardiovascular Disease: A Scientific Statement From the American Heart Association. *Circulat.* **143**, e984–e1010 (2021).
4. Vignini, A. et al. Alzheimer's disease and diabetes: new insights and unifying therapies. *Curr Diabet. Rev.* **9**, 218–227 (2013).
5. O'Brien, R. J. & Wong, P. C. Amyloid precursor protein processing and Alzheimer's disease. *Annu. Rev. Neurosci.* **34**, 185–204 (2011).
6. Chaney, M. O. et al. RAGE and amyloid beta interactions: atomic force microscopy and molecular modeling. *Biochim. et Biophys. Acta* **1741**, 199–205 (2005).
7. Tran, L., Basdevant, N., Prevost, C. & Ha-Duong, T. Structure of ring-shaped Abeta(4)(2) oligomers determined by conformational selection. *Sci. Rep.* **6**, 21429 (2016).
8. Xue, C. et al. Abeta42 fibril formation from predominantly oligomeric samples suggests a link between oligomer heterogeneity and fibril polymorphism. *R. Soc. Open Sci.* **6**, 190179 (2019).
9. Bharadwaj, P. et al. Role of the cell membrane interface in modulating production and uptake of Alzheimer's beta amyloid protein. *Biochim. Biophys. Acta Biomembr.* **1860**, 1639–1651 (2018).
10. Mark, R. J., Pang, Z., Geddes, J. W., Uchida, K. & Mattson, M. P. Amyloid beta-peptide impairs glucose transport in hippocampal and cortical neurons: involvement of membrane lipid peroxidation. *J. Neurosci.* **17**, 1046–1054 (1997).
11. Prapong, T. et al. Amyloid beta-peptide decreases neuronal glucose uptake despite causing increase in GLUT3 mRNA transcription and GLUT3 translocation to the plasma membrane. *Exp. Neurol.* **174**, 253–258 (2002).
12. Malkov, A. et al. Abeta initiates brain hypometabolism, network dysfunction and behavioral abnormalities via NOX2-induced oxidative stress in mice. *Commun. Biol.* **4**, 1054 (2021).
13. Casley, C. S., Canevari, L., Land, J. M., Clark, J. B. & Sharpe, M. A. Beta-amyloid inhibits integrated mitochondrial respiration and key enzyme activities. *J. Neurochem.* **80**, 91–100 (2002).
14. Moreira, P. I., Santos, M. S., Moreno, A. & Oliveira, C. Amyloid beta-peptide promotes permeability transition pore in brain mitochondria. *Biosci. Rep.* **21**, 789–800 (2001).
15. Mossmann, D. et al. Amyloid-beta peptide induces mitochondrial dysfunction by inhibition of preprotein maturation. *Cell Metabol.* **20**, 662–669 (2014).
16. Tillement, L., Lecanu, L. & Papadopoulos, V. Further evidence on mitochondrial targeting of beta-amyloid and specificity of beta-amyloid-induced mitotoxicity in neurons. *Neurodegener. Dis.* **8**, 331–344 (2011).
17. Roher, A. E. et al. Amyloid beta peptides in human plasma and tissues and their significance for Alzheimer's disease. *Alzheimer's Dement. J. Alzheimer's Associat.* **5**, 18–29 (2009).
18. Lee, Y. H. et al. Amyloid precursor protein expression is upregulated in adipocytes in obesity. *Obesity (Silver Spring)* **16**, 1493–1500 (2008).
19. An, Y. A. et al. Dysregulation of Amyloid Precursor Protein Impairs Adipose Tissue Mitochondrial Function and Promotes Obesity. *Nat. Metab.* **1**, 1243–1257 (2019).
20. Fujiwara, T., Oda, K., Yokota, S., Takatsuki, A. & Ikehara, Y. Brefeldin A causes disassembly of the Golgi complex and accumulation of secretory proteins in the endoplasmic reticulum. *J. Biol. Chem.* **263**, 18545–18552 (1988).
21. Balakrishnan, K. et al. Plasma Abeta42 correlates positively with increased body fat in healthy individuals. *J. Alzheimer's Dis. JAD* **8**, 269–282 (2005).
22. Fung, J., Frost, D., Chakrabartty, A. & McLaurin, J. Interaction of human and mouse Abeta peptides. *J. Neurochem.* **91**, 1398–1403 (2004).
23. Lopaschuk, G. D., Folmes, C. D. & Stanley, W. C. Cardiac energy metabolism in obesity. *Circulat. Res.* **101**, 335–347 (2007).
24. Rayner, J. J. et al. The relative contribution of metabolic and structural abnormalities to diastolic dysfunction in obesity. *Int J. Obes.* **42**, 441–447 (2018).
25. Borlaug, B. A. et al. Obesity and heart failure with preserved ejection fraction: new insights and pathophysiologic targets. *Cardiovasc. Res.* (2022).
26. Obokata, M., Reddy, Y. N. V., Pislaru, S. V., Melenovsky, V. & Borlaug, B. A. Evidence Supporting the Existence of a Distinct Obese Phenotype of Heart Failure With Preserved Ejection Fraction. *Circulation* **136**, 6–19 (2017).
27. Koenig, A. L. et al. Single-cell transcriptomics reveals cell-type specific diversification in human heart failure. *Nat. Cardiovasc. Res.* **1**, 263–280 (2022).
28. Yan, Y. & Wang, C. Abeta42 is more rigid than Abeta40 at the C terminus: implications for Abeta aggregation and toxicity. *J. Mol. Biol.* **364**, 853–862 (2006).
29. Hoglund, K. et al. Plasma levels of beta-amyloid(1-40), beta-amyloid(1-42), and total beta-amyloid remain unaffected in adult patients with hypercholesterolemia after treatment with statins. *Arch. Neurol.* **61**, 333–337 (2004).
30. Dunlay, S. M., Roger, V. L. & Redfield, M. M. Epidemiology of heart failure with preserved ejection fraction. *Nat. Rev. Cardiol.* **14**, 591–602 (2017).

31. Czeczor, J. K. et al. APP deficiency results in resistance to obesity but impairs glucose tolerance upon high fat feeding. *J. Endocrinol.* **237**, 311–322 (2018).
32. Meakin, P. J. et al. Reduction in BACE1 decreases body weight, protects against diet-induced obesity and enhances insulin sensitivity in mice. *Biochem. J.* **441**, 285–296 (2012).
33. Zago, W. et al. Neutralization of soluble, synaptotoxic amyloid beta species by antibodies is epitope specific. *J. Neurosci.* **32**, 2696–2702 (2012).
34. Salloway, S. et al. Two phase 3 trials of bapineuzumab in mild-to-moderate Alzheimer's disease. *New Engl J. Med.* **370**, 322–333 (2014).
35. Mureddu, G. F., de Simone, G., Greco, R., Rosato, G. F. & Contaldo, F. Left ventricular filling pattern in uncomplicated obesity. *Am. J. Cardiol.* **77**, 509–514 (1996).
36. Aljaroudi, W. et al. Impact of body mass index on diastolic function in patients with normal left ventricular ejection fraction. *Nutr. Diabetes* **2**, e39 (2012).
37. Ingul, C. B., Tjonna, A. E., Stolen, T. O., Stoylen, A. & Wisloff, U. Impaired cardiac function among obese adolescents: effect of aerobic interval training. *Arch. Pediatr. Adolesc. Med.* **164**, 852–859 (2010).
38. Gaur, V. et al. Scriptaid enhances skeletal muscle insulin action and cardiac function in obese mice. *Diab. Obes. Metabol.* **19**, 936–943 (2017).
39. Demattos, R. B. et al. A plaque-specific antibody clears existing beta-amyloid plaques in Alzheimer's disease mice. *Neuron* **76**, 908–920 (2012).
40. McFarland, T. M., Alam, M., Goldstein, S., Pickard, S. D. & Stein, P. D. Echocardiographic diagnosis of left ventricular hypertrophy. *Circulation* **57**, 1140–1144 (1978).
41. Hampel, H. et al. The Amyloid-beta Pathway in Alzheimer's Disease. *Mol. Psychiatry* **26**, 5481–5503 (2021).
42. Kaspi, A. & Ziemann, M. mitch: multi-contrast pathway enrichment for multi-omics and single-cell profiling data. *BMC Genom.* **21**, 447 (2020).
43. Boudina, S. et al. Reduced mitochondrial oxidative capacity and increased mitochondrial uncoupling impair myocardial energetics in obesity. *Circulation* **112**, 2686–2695 (2005).
44. Chatham, J. C. & Seymour, A. M. Cardiac carbohydrate metabolism in Zucker diabetic fatty rats. *Cardiovasc. Res.* **55**, 104–112 (2002).
45. Lewis, A. J., Neubauer, S., Tyler, D. J. & Rider, O. J. Pyruvate dehydrogenase as a therapeutic target for obesity cardiomyopathy. *Expert. Opin. Ther. Targets* **20**, 755–766 (2016).
46. Lustbader, J. W. et al. ABAD directly links Abeta to mitochondrial toxicity in Alzheimer's disease. *Science* **304**, 448–452 (2004).
47. Caspersen, C. et al. Mitochondrial Abeta: a potential focal point for neuronal metabolic dysfunction in Alzheimer's disease. *FASEB J* **19**, 2040–2041 (2005).
48. Schroeter, S. et al. Immunotherapy reduces vascular amyloid-beta in PDAPP mice. *J. Neurosci.* **28**, 6787–6793 (2008).
49. Bobba, A. et al. Mitochondrial respiratory chain Complexes I and IV are impaired by beta-amyloid via direct interaction and through Complex I-dependent ROS production, respectively. *Mitochondrion* **13**, 298–311 (2013).
50. Niemann, B. et al. Obesity induces signs of premature cardiac aging in younger patients: the role of mitochondria. *J. Am. Coll. Cardiol.* **57**, 577–585 (2011).
51. Montaigne, D. et al. Myocardial contractile dysfunction is associated with impaired mitochondrial function and dynamics in type 2 diabetic but not in obese patients. *Circulation* **130**, 554–564 (2014).
52. Ide, T. et al. Mitochondrial electron transport complex I is a potential source of oxygen free radicals in the failing myocardium. *Circulation Research* **85**, 357–363 (1999).
53. Sheeran, F. L. & Pepe, S. Posttranslational modifications and dysfunction of mitochondrial enzymes in human heart failure. *Am. J. Physiol. Endocrinol. Metabol.* **311**, E449–E460 (2016).
54. Zhu, F. et al. Plasma Amyloid-beta in Relation to Cardiac Function and Risk of Heart Failure in General Population. *JACC Heart Fail.* **11**, 93–102 (2023).
55. Meakin, P. J. et al. Elevated circulating amyloid concentrations in obesity and diabetes promote vascular dysfunction. *J. Clin. Invest.* **130**, 4104–4117 (2020).
56. Puig, K. L. et al. Amyloid precursor protein modulates macrophage phenotype and diet-dependent weight gain. *Sci. Rep.* **7**, 43725 (2017).
57. Weaver, D. F. Amyloid beta is an early responder cytokine and immunopeptide of the innate immune system. *Alzheimers Dement (N Y)* **6**, e12100 (2020).
58. Gopal, K. et al. Cardiac-Specific Deletion of Pyruvate Dehydrogenase Impairs Glucose Oxidation Rates and Induces Diastolic Dysfunction. *Front. Cardiovasc. Med.* **5**, 17 (2018).
59. Sidhu, S. et al. Tissue-specific pyruvate dehydrogenase complex deficiency causes cardiac hypertrophy and sudden death of weaned male mice. *Am. J. Physiol. Heart Circulat. Physiol* **295**, H946–H952 (2008).
60. Dai, C. et al. Lactate Dehydrogenase A Governs Cardiac Hypertrophic Growth in Response to Hemodynamic Stress. *Cell Rep.* **32**, 108087 (2020).
61. Cluntun, A. A. et al. The pyruvate-lactate axis modulates cardiac hypertrophy and heart failure. *Cell Metabol.* **33**, 629–648.e610 (2021).
62. Lewis, H. et al. Quantification of Alzheimer pathology in ageing and dementia: age-related accumulation of amyloid-beta(42) peptide in vascular dementia. *Neuropathol. Appl. Neurobiol.* **32**, 103–118 (2006).
63. Troncone, L. et al. Abeta Amyloid Pathology Affects the Hearts of Patients With Alzheimer's Disease: Mind the Heart. *J. Am. Coll. Cardiol.* **68**, 2395–2407 (2016).
64. Jang, S., Chapa-Dubocq, X. R., Parodi-Rullan, R. M., Fossati, S. & Javadov, S. Beta-Amyloid Instigates Dysfunction of Mitochondria in Cardiac Cells. *Cells* **11** (2022).
65. Worth, A. J., Basu, S. S., Snyder, N. W., Mesaros, C. & Blair, I. A. Inhibition of neuronal cell mitochondrial complex I with rotenone increases lipid beta-oxidation, supporting acetyl-coenzyme A levels. *J. Biol. Chem.* **289**, 26895–26903 (2014).
66. Vazquez, E. J. et al. Mitochondrial complex I defect and increased fatty acid oxidation enhance protein lysine acetylation in the diabetic heart. *Cardiovasc. Res.* **107**, 453–465 (2015).
67. Gonzalez-Barroso, M. M. et al. Fatty acids revert the inhibition of respiration caused by the antidiabetic drug metformin to facilitate their mitochondrial beta-oxidation. *Biochim. Biophys. Acta* **1817**, 1768–1775 (2012).
68. Louch, W. E., Sheehan, K. A. & Wolska, B. M. Methods in cardiomyocyte isolation, culture, and gene transfer. *J. Mol. Cell. Cardiol* **51**, 288–298 (2011).
69. Piquereau, J. & Ventura-Clapier, R. Maturation of Cardiac Energy Metabolism During Perinatal Development. *Front. Physiol* **9**, 959 (2018).
70. Liu, B. et al. Comparative study on isolation and mitochondrial function of adult mouse and rat cardiomyocytes. *J. Mol. Cell. Cardiol* **136**, 64–71 (2019).
71. Peikert, A. & Cunningham, J. W. Amyloid-beta and the Risk of Heart Failure: Cause or Only Association? *JACC Heart Fail.* **11**, 103–105 (2023).
72. Venardos, K., De Jong, K. A., Elkamie, M., Connor, T. & McGee, S. L. The PKD Inhibitor CID755673 Enhances Cardiac Function in Diabetic db/db Mice. *PLoS One* **10**, e0120934 (2015).

73. De Jong, K. A. et al. Loss of protein kinase D activity demonstrates redundancy in cardiac glucose metabolism and preserves cardiac function in obesity. *Mol. Metabol* **42**, 101105 (2020).
74. Lindsey, M. L., Kassiri, Z., Virag, J. A. I., de Castro Bras, L. E. & Scherrer-Crosbie, M. Guidelines for measuring cardiac physiology in mice. *Am. J. Physiol. Heart Circulat Physiol* **314**, H733–H752 (2018).
75. Esparza, T. J. et al. Soluble Amyloid-beta Aggregates from Human Alzheimer's Disease Brains. *Sci. Rep.* **6**, 38187 (2016).
76. Martin, S. D., Morrison, S., Konstantopoulos, N. & McGee, S. L. Mitochondrial dysfunction has divergent, cell type-dependent effects on insulin action. *Mol. Metabol* **3**, 408–418 (2014).
77. Wu, W. et al. Activation of Hippo signaling pathway mediates mitochondria dysfunction and dilated cardiomyopathy in mice. *Theranostics* **11**, 8993–9008 (2021).
78. Gaur, V. et al. Disruption of the Class IIa HDAC Corepressor Complex Increases Energy Expenditure and Lipid Oxidation. *Cell Rep.* **16**, 2802–2810 (2016).
79. Williams, D. et al. Abnormal mitochondrial L-arginine transport contributes to the pathogenesis of heart failure and rexoygenation injury. *PLoS One* **9**, e104643 (2014).
80. Martin, S. D. & McGee, S. L. A systematic flux analysis approach to identify metabolic vulnerabilities in human breast cancer cell lines. *Cancer Metabol.* **7**, 12 (2019).

Acknowledgements

The authors wish to thank Dr Tom Gumley, Assoc. Prof. John Amerena, Prof. Mark Hargreaves, Dr Sophie Hussey and Professor Roberto Cappai for their assistance with this study and helpful discussions. The authors also wish to thank members of the Metabolic Research Unit for helpful discussions and Dr Richard Woolley for his assistance with echocardiography. The authors would also like to thank the Deakin University Animal Services team for their assistance throughout this study. Aspects of this work were funded by grants from the National Health and Medical Research Council (GNT1027226), the Diabetes Australia Research Program (Y17G-MCGS), the Ramaciotti Foundation and Ambetex Pty Ltd to SLM.

Author contributions

Conceptualization, L.G.H., J.K.C. and S.L.M.; Methodology, L.G.H., J.K.C., T.C., J.B., K.A.D.J., M.C.R., A.J.G., K.V., S.D.M., S.T.B., K.A.M., K.F.H., M.M., M.Z. and S.L.M.; Resources, K.F.H., J.A.C., G.R.C., K.W., M.M., M.Z. and S.L.M.; Writing – original draft, S.L.M.; Writing – review and editing, all authors; Funding acquisition, S.L.M.

Competing interests

Ambetex Pty Ltd has submitted patents containing aspects of this work (PCT/AU2020/051254; PCT/AU2020/051348; PCT/AU2020/051350; PCT/AU2020/051353). LGH, JKC, JAC, GRC and SLM own equity in Ambetex Pty Ltd. The remaining authors declare no conflict of interests.

Additional information

Supplementary information The online version contains supplementary material available at https://doi.org/10.1038/s41467-023-44520-4.

Correspondence and requests for materials should be addressed to Sean L. McGee.

Peer review information *Nature Communications* thanks the anonymous, reviewers for their contribution to the peer review of this work. A peer review file is available.